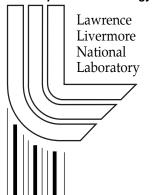


U.S. Department of Energy



M. W. A. Stewart, E. R. Vance, R. A. Day, and G. R. Lumpkin

April 10, 2000

This document was prepared as an account of work sponsored by an agency of the United States Government. Neither the United States Government nor the University of California nor any of their employees, makes any warranty, express or implied, or assumes any legal liability or responsibility for the accuracy, completeness, or usefulness of any information, apparatus, product, or process disclosed, or represents that its use would not infringe privately owned rights. Reference herein to any specific commercial product, process, or service by trade name, trademark, manufacturer, or otherwise, does not necessarily constitute or imply its endorsement, recommendation, or favoring by the United States Government or the University of California. The views and opinions of authors expressed herein do not necessarily state or reflect those of the United States Government or the University of California, and shall not be used for advertising or product endorsement purposes.

This work was performed under the auspices of the U.S. Department of Energy by University of California, Lawrence Livermore National Laboratory under Contract W-7405-Eng-48.

Interim Report, February 2000, to Lawrence Livermore National Laboratory for Contract B345772 –

Task 3: Immobilisation Process/Equipment Testing – Task 3.4: NonDestructive Evaluation

M.W.A. Stewart, E.R. Vance, R.A. Day and G.R. Lumpkin
10 April 2000

Materials Division
Australian Nuclear Science and Technology
Organisation
PMB 1, Menai NSW 2234
Australia

Task 3: Immobilisation Process/Equipment Testing –

Task 3.4: Non-Destructive Evaluation

Table of Contents

1	SUMMARY	1
•	EVDEDIMENTAL	2
2	EXPERIMENTAL	
	2.1 SAMPLE PREPARATION	
	2.1.1 Alkoxide-Route Wet-milled Powder Preparation	
	2.1.2 Oxide-Route Wet-milled Powder Preparation	
	2.1.3 Oxide-Route Dry-milled Powder Preparation	
	2.1.4 Attrition Milled Powder Preparation	
	2.1.5 Cold-pressing and Sintering	
	2.2 Analysis	
	2.2.1 X-ray Diffraction	
	2.2.2 Scanning Electron Microscopy	
	2.2.3 Transmission Electron Microscopy	10
3	RESULTS AND DISCUSSION	11
	3.1 Th/U-DOPED OXIDE-ROUTE SAMPLES	. 11
	3.1.1 Composition B1-2, Baseline Ceramic	. 11
	3.1.2 Composition B1-4, Baseline Ceramic + Impurities	
	3.1.3 Composition B1-10, Zirconolite-rich Ceramic	12
	3.1.4 Composition B1-12, Brannerite-rich Ceramic	13
	3.1.5 Composition B1-14, Nominally 10 % Perovskite Ceramic	13
	3.1.6 Composition B1-16, 10 % Phosphate Ceramic	14
	3.2 SUMMARY OF THE RESULTS ON THE Th/U-DOPED SAMPLES	. 14
	3.3 Pu-doped Samples	
	3.3.1 Composition B1-1, Baseline Ceramic	. 15
	3.3.2 Compositions A-7 and B3-13, Baseline Ceramic + Impurities	
	3.3.3 Composition B1-13, Nominally 10 % Perovskite Ceramic	
	3.4 SUMMARY OF THE RESULTS ON THE Pu/U-DOPED SAMPLES	
	3.4.1 Pu-doped Versus Th-doped Samples	
	3.5 IDENTIFICATION OF ADDITIONAL XRD PEAKS IN ZIRCONOLITE-BEARING SAMPLES	. 18
4	WORK IN PROGRESS	19
_	CONCENTATION	40
5	CONCLUSIONS	19
6	ACKNOWLEDGMENTS	20
	PPENDIX A: SCANNING ELECTRON MICROGRAPHS, ENERGY DISPERSIVE X-RAY PECTROMETRY, IMAGE ANALYSIS AND X-RAY DIFFRACTION RESULTS FOR SAMPLES OF	
	OMPOSITION B1-2 - Th/U-DOPED BASELINE CERAMIC	
	PPENDIX B: SCANNING ELECTRON MICROGRAPHS, ENERGY DISPERSIVE X-RAY	
	PECTROMETRY, IMAGE ANALYSIS AND X-RAY DIFFRACTION RESULTS FOR SAMPLES OF	
	OMPOSITION B1-4 - Th /U-DOPED BASELINE + IMPURITIES CERAMIC	
	PPENDIX C: SCANNING ELECTRON MICROGRAPHS, ENERGY DISPERSIVE X-RAY	
	PECTROMETRY, IMAGE ANALYSIS AND X-RAY DIFFRACTION RESULTS FOR SAMPLES OF OMPOSITION B1-10 - Th/U-DOPED ZIRCONOLITE-RICH CERAMIC	
	PPENDIX D: SCANNING ELECTRON MICROGRAPHS, ENERGY DISPERSIVE X-RAY	
	PECTROMETRY, IMAGE ANALYSIS AND X-RAY DIFFRACTION RESULTS FOR SAMPLES OF	
C	OMPOSITION B1-12 - Th /U-DOPED BRANNERITE-RICH CERAMIC	
	PPENDIX E: SCANNING ELECTRON MICROGRAPHS, ENERGY DISPERSIVE X-RAY	
	PECTROMETRY, IMAGE ANALYSIS AND X-RAY DIFFRACTION RESULTS FOR SAMPLES OF	
C	OMPOSITION B1-14 - Th/U-DOPED "NOMINALLY" 10 % PEROVSKITE CERAMIC	

APPENDIX F: SCANNING ELECTRON MICROGRAPHS, ENERGY DISPERSIVE X-RAY SPECTROMETRY, IMAGE ANALYSIS AND X-RAY DIFFRACTION RESULTS FOR SAMPLES OF COMPOSITION B1-16 - Th/U-DOPED \sim 10 % PHOSPHATE-DOPED CERAMIC

APPENDIX G: SCANNING ELECTRON MICROGRAPHS, ENERGY DISPERSIVE X-RAY SPECTROMETRY, IMAGE ANALYSIS AND X-RAY DIFFRACTION RESULTS FOR SAMPLES OF COMPOSITION B1-1 - Pu/U-DOPED BASELINE CERAMIC

APPENDIX H: SCANNING ELECTRON MICROGRAPHS, ENERGY DISPERSIVE X-RAY SPECTROMETRY, IMAGE ANALYSIS AND X-RAY DIFFRACTION RESULTS FOR SAMPLES OF COMPOSITION A-7 AND B3-13 - Pu/U-DOPED BASELINE + IMPURITIES CERAMICS

APPENDIX I: SCANNING ELECTRON MICROGRAPHS, ENERGY DISPERSIVE X-RAY SPECTROMETRY, IMAGE ANALYSIS AND X-RAY DIFFRACTION RESULTS FOR SAMPLES OF COMPOSITION B1-13 - Pu/U-DOPED "NOMINALLY" 10 % PEROVSKITE CERAMIC

1 Summary

This report contains a summary of the results generated for Task 3.4: Non-destructive Evaluation (a subtask of Task 3: Immobilisation Process/Equipment Testing). The aim of this task was to carry out X-ray diffraction (XRD) on selected samples from previous Task 1: Form Development work. (Purchase Order B345772, Lawrence Livermore National Laboratory). These XRD results were to be compared to the results obtained using quantitative scanning electron microscopy.

Selected samples made as part of Task 1.2 (Near Equilibrium Processing Requirements) were used ^{1,2} for this work. All but one of the compositions tested:

- baseline,
- baseline ceramic plus process impurities,
- zirconolite-rich,
- brannerite-rich.
- nominally ~ 10 % perovskite in addition to the normal baseline phases,
- ~ 10 % phosphate-doped batch,

formed the phases expected. The exception was the nominally ~ 10 % perovskite batch, which did not form perovskite. The baseline composition ceramics formed pyrochlore as the main phase with 10 – 20 vol. % brannerite and 3 – 5 vol. % Hf-doped rutile. When impurities were added, 2M zirconolite formed at the expense of pyrochlore. A glassy silicate phase also formed. The zirconolite-rich ceramics and brannerite-rich samples were respectively richer in zirconolite and brannerite than the baseline composition ceramics. The phosphate-doped samples were similar to the baseline samples except that they contained the additional phase whitlockite (nominally Ca₃(PO₄)₂). Small amounts (< 1 vol. %) of ThO₂ and PuO₂ were found in some of the samples tested. The results for the Pu-doped samples are similar to the Th/U-doped batches and produced samples with similar microstructures, which indicate that Th is a good surrogate for Pu in the microstructural context. The major difference between Th and Pu was that the Th-doped samples contain more ($\sim 5-10$ vol. %) brannerite and the pyrochlores typically contain fewer formula units of Th than Pu. This may either be due to a greater tendency of Th to form the brannerite phase with U or limitations on the solubility of Th in the pyrochlore structure due to its relatively large ionic radius^{3,4}. This latter point was borne out in the Task 1.1 single-phase work ⁵. ThTi₂O₆ was found to be relatively simple to make, but CaThTi₂O₇ did not form. The Pu, U and Th partitioned as

¹ M W A Stewart, E R Vance, R A Day and A Brownscombe, *Interim Report on Task 1.2: Near Equilibrium Processing Requirements*, ANSTO Materials Division Report No. R99m012, 1 April 1999, Materials Division, ANSTO, Lucas Heights, Australia.

² M W A Stewart, E R Vance, R A Day and A Brownscombe, *Second Interim Report on Task 1.2: Near Equilibrium Processing Requirements*, ANSTO Materials Division Report No. R00m012, 30th April 2000, Materials Division, ANSTO, Lucas Heights, Australia.

³ R.A. McCauley, New Pyrochlores of the Charge-Coupled Type, J. Solid State Chem., **33** 99-105 (1980).

⁴ R.A. McCauley, *Microstructural characteristics of pyrochlore formation*, J. Appl. Phys., **51** (1) 290-294 (1980).

⁵ ER Vance, ML Carter and ER Day, *Interim Report on Task 1.1: Single-Phase Sample Production*, ANSTO Materials Division Report No. R99m022, 20 April 1999, Materials Division, ANSTO, Lucas Heights, Australia.

expected – mainly into the pyrochlore, brannerite and zirconolite. The amounts in the minor phases, rutile and whitlockite are small.

Samples sintered in air were similar to those sintered in Ar, in terms of types of phases present; however, the compositions of these phases did vary with sintering atmosphere. For example, in most samples (all but the Th/U/Hf-baseline B1-2 composition samples) the pyrochlore and brannerite in the air sintered samples appear to contain more Ca than the pyrochlore and brannerite in the Ar sintered samples. This probably reflects charge compensation within the pyrochlore to allow for the higher average redox state of the U when sintered in air - there is probably more U⁺⁵ and/or U⁺⁶ present in the air sintered samples. The amount of brannerite appears to be slightly greater in the air sintered samples.

No major differences were observed between the surfaces and interiors of pellets. Some deficiency in rutile around large pores and in a thin surface region ($\sim 20~\mu m$ thick) of the pellet was observed in Th/U-doped baseline and zirconolite-rich samples.

The XRD analyses were consistent with the microstructures observed; though some possible orientation effects could be observed in the XRD patterns of some Th-doped samples. A peak at a d-spacing of ~ 0.56 nm was observed in the XRD patterns of the Th-doped samples that contained zirconolite. This peak was more intense in XRD patterns of the surfaces of these pellets and appeared in both air and Ar sintered materials.

EDS analyses of the interior and exterior regions of the cross section of several pellets were carried out. Th/U-doped samples of each of the six compositions were tested. These samples had been sintered in air and Ar. They included samples made via both the wet and dry ball milling, and attrition milling process routes. Samples of the Pu/U-doped baseline and baseline plus impurities composition were also tested to confirm the applicability of the results obtained on the Th/U-doped samples. No significant differences were observed in the EDS analyses across any of these sintered samples.

2 Experimental

2.1 Sample Preparation

The samples tested are given in Table 1. Batches of the compositions given in Tables 1 and 2 were made by alkoxide-route⁶, oxide-route wet-mill⁷ and oxide-route dry-mill methods⁸. The compositions of the samples are given in Tables 2 and 3 and the raw materials used are given in Tables 4 and 5. Most of the samples tested were oxide-route, to provide information more related to the planned plutonium immobilisation processing line.

2.1.1 Alkoxide-Route Wet-milled Powder Preparation

The alkoxide precursors were made as follows. The Ti and Hf alkoxides were mixed together and diluted to 50 % by adding anhydrous ethanol. The required (Table 3) non-radioactive chemicals (Table 3) were mixed together in deionised water and added to the alkoxides⁹. The batch was then shear mixed for 10 minutes. Uranyl nitrate and Pu nitrate solutions were added to the batch. After these additions, the batch was stirred and then dried.

The dried powder was placed an alumina container and calcined in air for 1 hour at 750 °C. The calcined powder was then treated by wet ball milling (water) for 16 hours with 10 mm diameter yttria stabilised zirconia media in a nylon (Th/U-doped) or rubber jars (Pu/U-doped). Some batches were milled for 4 hours to examine the effect of milling time on equilibrium. The milled slurry was dried at ~ 120 °C. The resulting cake was passed through an ~ 0.5 mm sieve prior to cold pressing.

2.1.2 Oxide-Route Wet-milled Powder Preparation

The oxide precursors were made as follows. The non-radioactive elements were mixed together in a plastic jar taken to the uranium laboratory where UO₂, and ThO₂ if the batch was a Th-doped batch, were added. For Pu-doped batches the PuO₂ was added in the Actinide Suite.

The blended powder was placed in an alumina crucible and calcined for 1 hour in air at 750 $^{\circ}$ C. The calcined powders were placed in rubber or nylon jars with 10 mm diameter yttria-stabilised zirconia media and wet ball milled in water for 16 hours. The milled slurry was dried at \sim 120 $^{\circ}$ C.

⁶ B.B. Ebbinghaus, Procedure SMP-55-98, Revision 1, Form Development Fabrication Procedure #3: Fabrication Process using Nitrates and Alkoxides, LLNL, Livermore, CA, June 21, 1998

⁷ B.B. Ebbinghaus, Procedure SMP-55-98, Revision 2, Form Development Procedure #1 for Fabricating Immobilized Ceramic Forms: Baseline Process using Wet Ball Milling, LLNL, Livermore, CA, June 21, 1998.

⁸ B.B. Ebbinghaus, Procedure SMP-55-98, Revision 1, Form Development Fabrication Procedure #2: Baseline Fabrication Process using Dry-milling, LLNL, Livermore, CA, June 21, 1998.

⁹ Amount of water is 4 times the weight of alkoxide.

Table 1: Samples Tested for Task 3.4

Composition	Description	Processing Route
		Route/Milling/Sint. Temp. (°C)/Sint. atmosphere \$
Th/U/Hf		
D1 2	11	
B1-2	baseline ceramic	oxide/wet ball/1350/Ar
B1-2	baseline ceramic	oxide/wet ball/1350/air
B1-2	baseline ceramic	oxide/dry ball/1350/air
B1-2	baseline ceramic	oxide/wet attrition/1350/air
B1-4	baseline ceramic + impurities	oxide/wet ball/1350/Ar
B1-4	baseline ceramic + impurities	oxide/wet ball/1350/air
B1-4	baseline ceramic + impurities	oxide/dry ball/1350/air
B1-4	baseline ceramic + impurities	oxide/wet attrition/1350/air
B1-10	zirconolite-rich	oxide/wet ball/1350/Ar
B1-10	zirconolite-rich	oxide/wet ball/1350/air
B1-10	zirconolite-rich	oxide/wet attrition/1350/air
B1-12	brannerite-rich	oxide/wet ball/1350/Ar
B1-12	brannerite-rich	oxide/wet ball/1350/air
B1-12	brannerite-rich	oxide/dry ball/1350/air
B1-12	brannerite-rich	oxide/wet attrition/1350/air
B1-14	"nominally" 10 % perovskite	oxide/wet ball/1350/Ar
B1-14	"nominally" 10 % perovskite	oxide/wet ball/1350/air
B1-16	~ 10 % phosphate	oxide/wet ball/1350/Ar
B1-16	~ 10 % phosphate	oxide/wet ball/1350/air
Pu/U/Hf		
B1-1	baseline ceramic	oxide/wet ball/1350/Ar
A-7	baseline ceramic + impurities	oxide/wet ball/1325/Ar
B3-13	baseline ceramic + impurities	oxide/wet ball/1325/Ar
B3-13	baseline ceramic + impurities	oxide/wet ball/1350/air
B1-13	"nominally" 10 % perovskite	alkoxide/wet ball/1350/Ar

^{\$} Ball milling was carried out for 16 hours (dry or wet), Attrition milling was carried out for 45 minutes. Samples were sintered for 4 hours at the sintering temperature.

Table 2: Th/U-doped compositions made for Task 1.2 (given as weight % oxides).

Batch No.	B1-2 Baseline	B1-4 Baseline + Impurities	B1-10 Zirconolite -rich	B1-12 Brannerite -rich	B1-14 ~ 10 % nominal perovskite	B1-16 ~ 10 % nominal phosphate
Components	(Wt. %)	(Wt. %)	(Wt. %)	(Wt. %)	(Wt. %)	(Wt. %)
~ ~		0.70		- 00		
CaO	9.99	9.50	9.26	5.89	12.07	11.64
Gd ₂ O ₃	7.98	7.59	6.61	6.34	7.98	8.53
HfO ₂	10.69	10.16	24.26	9.95	10.88	9.72
ThO ₂	11.62	11.09	9.35	12.68	12.04	12.73
UO2	23.77	22.60	15.44	28.04	20.83	21.43
TiO ₂	35.96	34.21	33.93	37.10	36.19	32.59
		0.40				
Al ₂ O ₃		0.48	1.13			
B2O3		0.16				
CaCl ₂		0.63				
CaF ₂		0.42				
Cr2O3		0.08				
Fe ₂ O ₃		0.14				
Ga ₂ O ₃		0.54				
K ₂ O		0.31				
MgO		0.42				
MoO ₂ \$		0.27				
Na ₂ O		0.13				
NiO		0.12				
P2O5						3.35
SiO ₂		0.44				
Ta ₂ O ₅		0.18				
WO ₂ \$		0.47				
ZnO		0.07				
Total	100.00	100.00	100.00	100.00	100.00	100.00

 $[\]$ Note that in air MoO $_3$ and WO $_3$ are the more likely forms of the molybdenum and tungsten oxides.

Table 3: Pu/U-doped compositions made for Task 1.2 (given as weight % oxides).

Batch No.	B1-1 Baseline	B1-3 (A-9) Baseline +	A-7 Baseline + Impurities	B3-13 Baseline + Impurities	B1-13 ~ 10 % nominal
	i	Impurities	•	•	perovskite
Components	(Wt. %)	(Wt. %)	(Wt. %)	(Wt. %)	(Wt. %)
CaO	9.95	9.47	9.81	8.30	12.07
Gd ₂ O ₃	7.95	7.56	7.83	7.52	7.66
HfO ₂	10.65	10.13	10.50	10.27	10.88
PuO ₂	11.89	11.35	11.71	11.20	12.36
UO ₂	23.69	22.54	23.34	22.31	20.83
TiO ₂	35.87	34.11	35.33	33.80	36.19
Al ₂ O ₃		0.48	0.32	0.73	
B ₂ O ₃		0.16	0.32	0.10	
CaCl ₂		0.63	0.16	0.67	
CaF ₂		0.42	0.10	1.03	
Cr ₂ O ₃		0.08	0.02	0.05	
Fe ₂ O ₃		0.03	0.02	0.03	
FeO		0.14	0.08	0.19	
Ga ₂ O ₃		0.54	0.14	0.19	
K2O		0.30	0.07	0.22	
MgO		0.42	0.07	0.43	
MoO ₂ \$		0.42	0.13	0.16	
Na ₂ O		0.13	0.06	0.23	
NiO		0.13	0.04	0.09	
P ₂ O ₅		0.12	0.04	0.006	
SiO ₂		0.44	0.19	0.88	
Ta ₂ O ₅		0.18	0.06	0.08	
WO ₂ \$		0.47	5.00	0.02	
ZnO		0.07	0.01	0.06	
BaO		3.07	0.01	0.14	
CeO ₂				0.18	
CuO ₂				0.11	
La ₂ O ₃				0.02	
Nd ₂ O ₃				0.29	
PbO				0.52	
Total	100.00	100.00	100.00		100.00
1 Olai	100.00	100.00	100.00		100.00

 $[\]$ Note that in air MoO $_3$ and WO $_3$ are the more likely forms of the molybdenum and tungsten oxides.

Table 4: Raw materials used for the alkoxide batches.

Element	Raw Materials (raw material, source, catalogue number)				
Ca	99 % Ca(NO ₃) ₂ .4H ₂ O, Aldrich Chem. Co., 23712-4				
Gd	99.9 % Gd(NO ₃) ₃ .6H ₂ O, Aldrich Chem., 21159-1				
Hf	99.99 % Hafnium n-butoxide, Gelest Inc.				
Pu	Pu nitrate solution, (Pu-239) made by dissolving PuO ₂ in 8M HNO ₃ .				
U	UO ₂ (NO ₃) ₂ .6H ₂ O, depleted (~ 0.318 % U235), BDH, Batch FF296, 10289				
Ti	Titanium isopropoxide, HÜLS Troisdorf Gmb., 405514				

Table 5: Raw materials used for the oxide batches.

Element	Raw Materials (raw material, source, catalogue number)					
Ca	Ca(OH) ₂ , AR grade, BDH Ltd. 90131					
Gd	99.9 % Gd ₂ O ₃ , Fairmount Chem., B913.00.40 and 99.9 % -325 mesh Gd ₂ O ₃ , Cerac					
	Speciality Inorganics, G-1015					
Hf	99.95 % HfO ₂ , -325 mesh, Cerac Speciality Inorganics, H-1011					
Pu	Pu nitrate solution, (Pu-239) made by dissolving PuO ₂ in 8M HNO ₃ .					
Th	Calcined (1050°C) Th(NO ₃) ₄ .5H ₂ O, Merck, 1.08162					
U	Calcined 1050°C, UO ₂ (NO ₃) ₂ .6H ₂ O, depleted (~ 0.318 % U235), BDH, Batch FF296,					
	10289					
Ti	> 99.1 % TiO ₂ , pigment grade anatase, Tioxide Pty. Ltd., AHR select 100375. This					
	contains ~ 0.4 wt. % P_2O_5 , 0.02 wt. % ZrO_2 , 0.01 wt. % CaO and a trace of K and Ce.4					
Al	99.6 % Al ₂ O ₃ , Degussa AG, Aluminium Oxide C					
В	H ₃ BO ₃ , Ajax Chem., Unilab 102					
Cl	CaCl ₂ , BDH, AR grade 27587,					
Cr	Cr ₂ O ₃ , BDH, AR grade 218330					
F	CaF ₂ , BDH, AR grade 540823					
Fe	99 % + Fe ₂ O ₃ , Aldrich Chem., 31005-0					
Ga	99.999 % Ga ₂ O ₃ , Chemat Tech., RG-304					
K	KOH, Merck, 5033					
Mg	MgO, Johnson Matthey, Specpure J.M. 130					
Mo	99.995 % MoO ₃ , BDH, 16669 or MoO ₃ , Johnson Matthey, Specpure J.M. 726					
Na	NaOH, Merck, 6498					
Ni	NiO, Johnson Matthey, Specpure J.M. 895					
P	85% H ₃ PO ₄ , Ajax Chem.,					
Si	Ludox HS-40 colloidal silica, 40% suspension in water, Aldrich Chem., 42081-6					
Та	99.9 % Ta ₂ O ₅ , A.D. MacKay Ltd.					
W	99.9 % WO ₃ , BDH, 30543					
Zn	99.9 % ZnO, Aldrich Chem., 20553-2					
Ba	Ba(OH) ₂ .8H ₂ O, Fluka, 11781					
Ce	99.9 % CeO ₂ , < 5 micron, Aldrich Chem Co., 21,157-5					
La	La ₂ O ₃ , Johnson Matthey, Specpure J.M. 303					
Nd	Nd ₂ O ₃ , Johnson Matthey, Specpure J.M. 321					
Pb	Pb ₃ O ₄ , Aldrich, 24,154-7					

2.1.3 Oxide-Route Dry-milled Powder Preparation

The blended oxide-route powders were made as in the preceding section and calcined in an alumina container for 1 hour at 750°C in air.

The calcined powders, jars¹⁰ and media were dried at ~ 120°C prior to dry ball milling. Dry ball milling was carried out in rubber (Pu/U-doped) or nylon jars (Th/U-doped) with 10 mm diameter yttria-stabilised zirconia media for 16 hours.

The dry milled baseline powder (B1-2) from previous work was remilled ¹. The aim was to see if the amount of agglomeration/heterogeneity in the original sample could be reduced. In this previous work 16 hours of dry ball milling, using a nylon jar with 10 mm diameter zirconia balls, was found to result in the formation of a "hard" cake on the jar and balls. The remaining powder batch (~ 15 g) was milled for 16 hours with 4 drops of alcohol. At the end of this time a hard cake still formed on the mill and on the grinding balls. The cake was broken up with a spatula and the samples were milled again for 16 hours, with 10 drops of alcohol. A cake again formed on the mill walls, but the grinding balls had less powder attached. The cake was broken up and another 10 drops of alcohol were added. A small amount of caking still occurred on the walls. This cake was not as hard and compacted as earlier mills and was easy to remove. The grinding balls were clean.

2.1.4 Attrition Milled Powder Preparation

Attrition milling methods and results are discussed in detail elsewhere ². The attritor is a Union Process 01-HDT machine that has been modified for use inside a glovebox. Milling was carried out in a 110 cc polyethylene quick-change pot. Approximately 140 g of 2mm diameter yttria-stabilised zirconia media were used. Milling was done at 450 rpm for 45 minutes. Approximately 15 ml of deionised water was added to the mill for wet milling. The batch size in both cases was ~ 10 g. After wet milling the media were separated from the slurry by a sieve. Water was used to wash the remaining slurry from the media and pot. The media and pot were then thoroughly cleaned and dried before dry milling the next composition.

The Th/U-doped powders were made via the oxide-route using "high-fired" ThO₂ and UO₂- 1050° C for 4 hours, in air for ThO₂ and Ar for UO₂. In earlier attrition mill runs it was noticed that large (~ $500 \,\mu$ m) lumps of black UO₂ and white ThO₂ were present in the dry and wet milled powders and that samples made from this material were inhomogeneous. Hence for these batches the "high-fired" ThO₂ and UO₂ were premilled prior to addition to the batches. This was done by wet ball milling for $16 \, \text{hours}$ in nylon jars with $10 \, \text{mm}$ diameter yttria-stabilised zirconia media. Water was used in milling the ThO₂ and iso-propanol for the UO₂.

The attrition milled powders were calcined at 750°C in air.

 $^{^{10}}$ Rubber milling jars were not dried at \sim 110-120°C, but were cleaned with alcohol and air dried at room temperature prior to milling.

2.1.5 Cold-pressing and Sintering

Pellets were prepared by cold pressing the powders in steel dies at ~ 60 MPa. Dies were lubricated with oleic acid. Pellets of 10 or 20 mm diameter were made for this work.

Batches B1-14 and B-16, made via the oxide-route, laminated during the initial pressing runs. Therefore, PEG 400 was added to these batches as a binder/lubricant, to eliminate the laminations. This PEG was added to the powder just prior to pressing, using a mortar and pestle for mixing.

The green pellets were sintered in an alumina tube furnace. Sintering atmospheres used were air (open furnace tube ends) or 0.25 l/min. of Ar. The sintering time was 4 hours. The standard sintering temperature was 1350 °C with selected samples being fired between 1300 and 1400 °C. The heating and cooling rates were 5 °C/min.

2.2 Analysis

2.2.1 X-ray Diffraction

X-ray diffraction (XRD) was carried out using either a Siemens D500 diffractometer employing Co K-alpha radiation, or a Scintag X1 Advanced Diffractometer System, with Cu K-alpha radiation.

The Pu/U-doped samples were mounted in resin and polished to a 0.25- $1.0~\mu m$ diamond finish. XRD was carried out on this polished surface.

XRD was carried out on various regions of the Th/U-doped samples: (a) the as-sintered top surface of the pellet; (b) the as-sintered bottom surface of the pellet; (c) the ground face of the pellet; and, (d) a small sample of powder from the pellet. The powder XRD patterns were obtained was done with and/or without tungsten metal as an internal reference standard. This powdered sample was a thin film on a resin base. Some samples were also done on a "zero-background" silicon base, which gave no Bragg scattering when run in the theta -2 theta mode. The aim is to reduce the interference effects of the broad background peaks at $\sim 20 - 25^{\circ}$ 2-theta from the epoxy resin and to obtain satisfactory XRD patterns with the minimum amount of radioactive contaminated powder.

Quantitative XRD was carried out on a selected Pu-doped sample using Rietveld Analysis software¹¹. Further work will be carried out on additional samples.

2.2.2 Scanning Electron Microscopy

The samples were examined by scanning electron microscopy (SEM) using either JEOL JSM6400 or JEOL JSM6300 machines, both of which are fitted with energy dispersive x-ray spectrometry (EDS) instruments for quantitative analysis.

Image analysis was carried out manually, using visual estimation diagrams to determine the percentages of the various components present. On selected samples quantitative analysis was carried out on grains inside the sample and grains near (within $\sim 20~\mu$ m) the edge of the sample.

_

¹¹ SIROQUANT version 1.0, CSIRO, Melbourne, Australia.

The SEM images of selected samples were examined by digital techniques using image analysis software ¹². An ANSTO macro developed for this software was used to determine the amount of each phase present. Conventional density slicing techniques did not work effectively with images of the samples tested due to contrast variations across the image.

2.2.3 Transmission Electron Microscopy

Grains of zirconolite were examined using a JEOL 2000FXII transmission electron microscope (TEM) operated at $200\,\mathrm{kV}$ and $120\,\mu\mathrm{A}$ beam current. The instrument was calibrated for electron diffraction work over a range of objective lens current settings using a Au standard. Selected area diffraction patterns were obtained at various tilt angles using a JEOL double tilting specimen holder. This holder is also designed for low background, analytical work. Diffraction patterns were obtained using a nominal camera length of 83 cm and an objective lens current settings of 7.010 and 6.972.

Energy dispersive X-ray (EDX) analyses were obtained using a Link ISIS Si(Li) solid state detector and multichannel analysis system. This system employs a digital top hat filter to suppress background, multiple least squares fitting of library spectra to obtain the peak counts, and a Cliff-Lorimer thin film procedure to reduce the data to oxide weight percent. We use empirical k-factors determined from a large suite of synthetic and natural reference materials.

12 Scion Image Version 1.62 (Public Domain), by Wayne Rasbut, National Institutes of Health, USA, Scion Corp., USA, nih-image@soils.umn.edu.

-

3 Results and Discussion

The images from the SEM analyses are given, EDS analysis results and a summary of the XRD results are given in Appendices A to I. Electronic copies of the raw data files are included on a disk with this report.

3.1 Th/U-doped Oxide-route Samples

3.1.1 Composition B1-2, Baseline Ceramic

The results of SEM/EDS, XRD and image analysis of samples made from this composition are given in Appendix A. The estimated amount of each phase, done manually with the aid of visual estimation diagrams, is given in the EDS Tables A1 to A4.

The samples all had similar mineralogy, being composed of:

- $\sim 65 75 \text{ vol } \% \text{ pyrochlore}$
- $\sim 15 30$ vol. % brannerite
- $\sim 3 7$ vol. % rutile

Submicron ThO₂ (< 1 vol. %) was also present in some of the larger brannerite regions. A trace (<< 1 vol. %) of whitlockite¹³ was also found in some samples. Some (< 5 vol. %) 4M zirconolite was detected in the wet ball milled sample sintered in Ar at 1350 °C: this could be due to incomplete milling leading to localised inhomogeneity in the green state, or incomplete reaction on sintering. Sintering in air resulted in a slight (< 5 vol. %) increase in the amount of brannerite present and this was observed in the XRD pattern (Appendix A, A.3.2).

The sintered dry ball milled sample tested had a different microstructure to a previously reported dry ball milled sample ¹. The current sample was prepared by re-milling the previously dry milled powder, but breaking up the cake every 16 hours and using isopropyl alcohol to aid milling (see section 2.1.3). The result was a much more homogeneous sintered sample (fig. A-3). This sample, which had been sintered in air, also contained more brannerite than the equivalent wet ball milled sample sintered in Ar.

The attrition milled sample was also similar to the other samples, but contained slightly more rutile ($\sim 2 \text{ vol. }\%$). Some large lumps of rutile were detected in the sample (fig. A-4), indicating that the attrition milling was not as efficient as the wet ball milling. "Coarse" agglomerates of high-fired ThO₂ and UO₂ were observed in the green powder.

The compositions of the phases in the different samples were similar (Tables A-1 to A-4). In addition the compositions of the phases across the samples were also similar. The only major difference between the exterior and interior of the samples appears to be a thin (\sim 20 μ m) layer at the surface of the pellet which appears to be deficient in rutile (figs. A-2(a), A-3 (a) and (c), A-4 (b)

-

 $^{^{13}}$ The whitlockite occurs due to trace phosphorus impurity in the anatase raw material.

and (d)). This difference was not picked up in the XRD, probably due to the small amount of rutile present (< 5 vol. %).

3.1.2 Composition B1-4, Baseline Ceramic + Impurities

The results of SEM/EDS, XRD and image analysis of samples made from this composition are given in Appendix B. The estimated amount of each phase, done manually with the aid of visual estimation diagrams, is given in the EDS Tables B1 to B4.

The samples all had similar mineralogy, being composed of:

- ~ 55 80 vol % pyrochlore
- $\sim 10 15$ vol. % 2M zirconolite
- $\sim 10 25$ vol. % brannerite
- < 1 ~ 5 vol. % rutile

Submicron Th/U-oxide (< 1 vol. %) was also present in some of the larger brannerite regions. Some "unreacted" hafnia (typically < 1 μ m in diameter) was found inside some of the zirconolite grains in the dry milled sample. Sintering in air may have resulted in a slight (~ 5 vol. %) increase in the amount of brannerite present (Table B1 and B-2). The dry ball milled sample had more brannerite and was much less homogeneous. The attrition milled sample had more and coarser rutile grains present.

No major difference was observed between the compositions of the phases at the interior and exterior of the pellets.

An additional XRD peak at ~ 0.56 nm was observed in the XRD pattern. This peak was more intense in the XRD patterns of the surfaces of the pellets (Appendix B, B.3). Preferred orientation of the zirconolite crystals at the surface may also be occurring. The deficiency in rutile near the surface of the sample, observed in the baseline B1-2 composition samples, was not observed in these samples.

3.1.3 Composition B1-10, Zirconolite-rich Ceramic

The results of SEM/EDS, XRD and image analysis of samples made from this composition are given in Appendix C. The estimated amount of each phase, done manually with the aid of visual estimation diagrams, is given in the EDS Tables C1 to C3.

The samples all had similar mineralogy, being composed of

- $\sim 40 50 \text{ vol } \%$ pyrochlore
- ~ 30 50 vol. % 2M zirconolite
- $\sim 10-20$ vol. % brannerite
- < 1 ~ 7 vol. % rutile

Submicron Th/U-oxide (< 1 vol. %) was also present in some of the larger brannerite regions.

The attrition milled sample had more and coarser rutile grains present, but is denser than the wet ball milled samples.

No major differences were observed between the interior and exterior compositions of the phases in

the pellets. Occasional variations in brannerite composition were observed, due to heterogeneous starting powders with localised concentrations of ThO₂ or UO₂ in the green pellet.

A thin (\sim 20 μ m) layer at the surface of some pellets appears to be deficient in rutile (fig. C-3). An additional XRD peak at \sim 0.56 nm was observed in the XRD pattern. This peak was more intense in the XRD patterns of the surfaces of the pellets (Appendix C, C.3). Orientation of the zirconolite crystals at the surface may also be occurring. In particular there is a difference between the XRD patterns of the top and bottom of the pellets. The tops and bottoms of the pellets have more intense zirconolite peaks and less intense rutile peaks than the ground faces or powdered samples.

The attrition milled sample (sintered in air) is deficient in brannerite in the outer 20 - 50 µm (fig. C-3 and section C.3.3). This was not observed in the wet ball milled samples but these were very porous (figs. C-1 and C-2), whereas the attrition milled samples has a low open porosity (fig. C-3).

3.1.4 Composition B1-12, Brannerite-rich Ceramic

The results of SEM/EDS, XRD and image analysis of samples made from this composition are given in Appendix C. The estimated amount of each phase, done manually with the aid of visual estimation diagrams, is given in the EDS Tables D1 to D4.

The samples all had similar mineralogy, being composed of:

- ~ 45 55 vol % pyrochlore
- ~ 45 55 vol. % brannerite
- < 1 ~ 5 vol. % rutile

Fine Th/U-oxide (< 1 vol. %) was also present in some of the larger brannerite regions. A few large grains of zirconolite were observed in the wet ball milled sample sintered in air. This may be due to inhomogeneity in the green pellet/powder or due to a trace of Al process contamination in the sample.

The dry milled sample is heterogeneous. The attrition milled sample had more and coarser rutile grains present than the wet ball milled samples.

No major differences were observed between the interior and exterior compositions of the phases in the pellets. Occasional variations in brannerite composition were observed, due to lumps of residual ThO_2 or UO_2 in the green powder. The 20 μ m layer deficient in rutile was not observed.

3.1.5 Composition B1-14, Nominally 10 % Perovskite Ceramic

The results of SEM/EDS, XRD and image analysis of samples made from this composition are given in Appendix E. The estimated amount of each phase, done manually with the aid of visual estimation diagrams, is given in the EDS Tables E1 to E4.

The samples all had similar mineralogy, being composed of:

- ~ 80 95 vol % pyrochlore
- $\sim 0 10$ vol. % brannerite
- ~ 5 10 vol. % rutile

The major phase difference between the Ar and air sintered samples was the presence of brannerite in the air sintered sample, but not in the Ar sintered sample. The pyrochlore of the air sintered sample was also richer in Ca than the air sintered sample.

No difference between the outside and inside of the samples was observed. The compositions and phase abundances were similar.

3.1.6 Composition B1-16, 10 % Phosphate Ceramic

The results of SEM/EDS, XRD and image analysis of samples made from this composition are given in Appendix F. The estimated amount of each phase, done manually with the aid of visual estimation diagrams, is given in the EDS Tables F1 to F4.

The samples all had similar mineralogy, being composed of:

- ~ 75 85 vol % pyrochlore
- $\sim 0 10$ vol. % brannerite
- ~ 5 10 vol. % whitlockite
- ~ 1 vol. % rutile

A trace of Th/U-oxide was also detected as small regions inside some brannerite grains. The Ar sintered sample was more porous than the air sintered sample. The brannerite and pyrochlore of the air sintered sample were also richer in Ca than the air sintered sample.

No difference between the outside and inside of the samples was observed. The compositions and phase abundances were similar.

3.2 Summary of The Results on the Th/U-doped Samples

The types of phases present in the sintered samples do not appear to be significantly affected by the sintering atmosphere, e.g., pyrochlore, brannerite, and rutile are found in the baseline composition sintered in both air and Ar. The composition of the individual phases can however vary with sintering atmosphere. For example, in most samples (all but the baseline B1-2 composition samples) the pyrochlore and brannerite contain more Ca in their formula than in the Ar sintered samples. This probably reflects charge compensation within the pyrochlore and brannerite to allow for the higher redox state of the U when sintered in air - some U⁺⁵ is most likely present in the air sintered samples. Vance, et al., ^{14,15} have examined Uranium-doped titanates sintered under various redox conditions using diffuse reflectance spectroscopy and XANES and found evidence of U⁺⁵ in air sintered zirconolites and brannerites.

The only free (Th,U)O₂ found in the samples made from the wet ball milled powders was located in the centre of some brannerite grains at both the interior and exterior of the pellets.

¹⁴ M.L. Carter, E.R. Vance, G.R. Lumpkin and B.D. Begg, *The CaZrTi*₂O₇ - CaUTi₂O₇ Phase Diagram, p. 63 – 64 in HLW and Pu immobilization meeting Abstracts, INSTN – Saclay, France, April 22/23, 1999, ed. C. Meis, DCC/DPE/SPCP, Saclay, 1999.

E.R. Vance, J.N. Watson, M.L. Carter, R.A. Day, G.R. Lumpkin, K.P. Hart, Y. Zhang, P.G. McGlinn, M.W.A. Stewart and D.J. Cassidy, Crystal Chemistry, Radiation Effects and Aqueous Leaching of Brannerite, UTi₂O₆, in Symposium - Waste Management Science and Technology in the Ceramics and Nuclear Industries at the American Ceramic Society Annual Meeting, Indianapolis, April 25-28, 1999, in press 2000.

Dry ball milled samples are less homogeneous and have a larger grain size than the wet-milled samples and had more free (Th,U)O₂ than the wet-milled materials.

No significant variations were detected between the compositions of the individual phases at the exterior and interior of the pellets tested. Brannerite could be an unreliable indicator of phase compositional variation through a pellet as large variations in the brannerite composition could occur from grain to grain. This is a result of the presence of "coarse" agglomerates of high-fired ThO_2 or UO_2 in the green powder. Some deficiency in rutile around large pores and in a thin surface region (~ $20~\mu m$) of the pellet were observed in the Th/U-doped baseline and zirconolite-rich samples. A brannerite deficiency was also observed at the surface of the dense zirconolite-rich sample sintered in air that had been made via attrition milling.

The only major difference in the XRD patterns found between the exterior and interior was an XRD peak at ~ 0.56 nm in samples that contained zirconolite. This peak appears to be more prevalent near the surface and is limited to those samples sintered in air that contain zirconolite. Glancing incidence XRD was carried out and the peak remained in the XRD pattern, so the peak was not due to large aligned crystallites. The peak appears to be in the wrong spot for the 2M or 4M zirconolite super-lattice reflection (~ 0.575 nm). We suspected that the reflection may be a 3T zirconolite super-lattice reflection, but further TEM work was required to prove this (see section 3.5). Some preferred orientation effects on of brannerite and pyrochlore were also observed in XRD patterns taken of the surfaces of the pellets.

3.3 Pu-doped Samples

3.3.1 Composition B1-1, Baseline Ceramic

The results on pellets made of this composition have been discussed in a previous report ¹. The results presented here include those from a new batch of pellets made for leach testing (Task 2.1).

The results of SEM/EDS, XRD and image analysis of samples made from this composition are given in Appendix G. The estimated amount of each phase, done manually with the aid of visual estimation diagrams, is given in the EDS Tables G1.

Visually this sample was estimated to contain:

- $\sim 75 85$ vol. % pyrochlore
- ~ 10 15 vol % Pu/U-brannerite
- ~ 5 10 vol. % Hf-doped rutile
- < 1 vol. % (Pu,U)O₂, located within the brannerite grains

There is no difference between this sample and that made in 1997 ¹. No difference in phase composition or phase distribution was detected across the sample. The SEM and XRD results are consistent. Phase distribution analysis, as determined by electronic image analysis, is given in Table 6.

samples.

Sample	Pu68 (B1-1)		Pu75 (A-7)		Pu105 (B1-13)			
	Baseline		Baseline + Impurities		Nominally 10 % Perovskite			
					(Pyrochlore + Rutile)			
Phase	Composition (Vol. %)							
	With Pores	Solid	With Pores	Solid	With Pores	Solid		
Pyrochlore	73.7	79.3	62.8	66.3	88.8	98.3		
Brannerite	8.7	9.4	12.3	13.0				
2M Zirconolite			13.4	14.0				
Rutile	10.4	11.2	5.7	6.0	1.5	1.7		
(Pu,U)O ₂	0.1	0.1	0.1	0.2				
Silicate			0.4	0.5				
Porosity	7.1	-	5.3	-	9.7			
Total	100.0	100.0	100.0	100.0	100.0	100.0		

3.3.2 Compositions A-7 and B3-13, Baseline Ceramic + Impurities

The results of SEM/EDS, XRD and image analysis of samples made from this composition are given in Appendix H and Table 6. The estimated amount of each phase, done manually with the aid of visual estimation diagrams, is given in the EDS Tables H1 to H3. Electronic image analysis results are given in Table 6.

Two compositions were tested, viz, A-7 and B3-13. Composition B3-13 is a modified form of A-7 and contains more impurity elements (Table 3). The samples with impurities typically consisted of:

- $\sim 60 75$ vol. % pyrochlore
- ~ 10 15 vol. % brannerite
- ~ 10 15 vol. % 2M zirconolite
- ~ 5 7 vol. % Hf-doped rutile
- <1 ~2 vol. % of a silicate glassy phase (Si-Ca-Mg-Na-K-Ti-Al-Ga-O), probably a glass
- < 1 vol. % (Pu,U)O₂, located within the brannerite grains

In the B3-13 samples the composition of the phases across the air and Ar sintered pellets (top to bottom) were measured. No difference in composition was noted across these samples (Tables H2 and H3). The phases present and their composition in the top middle and bottom of each of the

pellets were similar (figs. H2- H-7, Tables H-2 and H-3). The phases present in both the air and Ar sintered samples were similar, though their compositions were different (Tables H2 and H3). The samples sintered in air had more formula units of Ca in the brannerite and pyrochlore.

3.3.3 Composition B1-13, Nominally 10 % Perovskite Ceramic

The results of SEM/EDS, XRD and image analysis of samples made from this composition are given in Appendix I and Table 6. The estimated amount of each phase, done manually with the aid of visual estimation diagrams, is given in the EDS Table I-1. Electronic image analysis results are given in Table 6. The SEM and XRD results are consistent. No variations in phase composition or distribution were observed across the SEM sample.

This sample, that has been sintered in Ar, at 1350 °C for 4 hours, contains pyrochlore plus ~ 1-2 vol. % rutile. No perovskite was detected. The additional Ca present in this formulation (compared to the baseline composition, Table 3) has been taken up by the pyrochlore. This formation of pyrochlore has been at the expense of brannerite, which was not detected in this sample. Based on our work with Th/U-doped samples ¹, brannerite is more likely to form if the samples are sintered in air.

3.4 Summary of The Results on the Pu/U-doped Samples

The XRD and SEM results of the Pu-doped samples were consistent. The baseline composition formed pyrochlore, brannerite and rutile. The addition of impurities resulted in the formation of 2M zirconolite and a minor silicate phase. The nominally 10 % perovskite composition did not produce perovskite; instead the additional Ca (relative to the baseline composition) was taken up by the pyrochlore.

A detailed analysis of the top, bottom and middle of pellets of composition B3-13 sintered in air and Ar yielded no difference between the phase composition across the pellets. The phases present in the air and Ar sinters were similar, however their compositions were different; the brannerite and pyrochlore contained more formula units of Ca.

3.4.1 Pu-doped Versus Th-doped Samples

The results of the Pu-doped samples are similar to the Th/U-doped batches and produced samples with similar microstructures, indicating that Th is a satisfactory surrogate for Pu in the microstructural context.

The major difference between Th and Pu was that the Th has a greater tendency to form brannerite. For example, In the baseline ceramic the U:Th and U:Pu ratios are 2:1 (in the bulk composition); however, the U:Th ratio in the brannerites formed was closer to unity. This results in the Th-doped pyrochlore in the baseline ceramics being slightly deficient in Th (relative to the Pu/U-doped ceramics). Similar trends occur in the other compositions. An extreme example of the effect of this difference between Th and Pu is in the ~ 10 % nominal perovskite batch. In the Th/U-doped batch the phases formed were pyrochlore, brannerite, Hf-doped rutile and some (Th,U)O₂ (the latter was only present in the in the oxide-route batches), whereas in the Pu/U-doped batch no brannerite formed. The phases formed in the latter were pyrochlore, Hf-doped rutile and some PuO₂. The PuO₂, which usually contains some U, was only present in the oxide-route samples in amounts of < 1 vol. %. Typically the Th-doped samples have $\sim 5-10$ vol. % more brannerite present.

3.5 Identification of Additional XRD Peaks in Zirconolite-bearing Samples

An additional peak was identified at ~ 0.557 nm in samples containing zirconolite; the zirconoliterich and the baseline plus impurities compositions (see Appendices B and C). A zirconoliterich sample was analysed by TEM

Several thin zirconolite crystals suitable for microanalysis and tilting experiments were located. TEM-EDX analyses of the crystals showed a range of compositions:

- 1 Ca_{0.94}Gd_{0.20}U_{0.24}Th_{0.07}Hf_{0.67}Ti_{1.89}O₇
- 2 Ca_{0.88}Gd_{0.14}U_{0.11}Th_{0.04}Hf_{0.92}Ti_{1.88}O₇
- 3 Ca_{0.75}Gd_{0.16}U_{0.10}Th_{0.04}Hf_{0.76}Ti_{2.10}O₇
- 4 Ca_{0.86}Gd_{0.19}U_{0.15}Th_{0.05}Hf_{0.82}Ti_{1.89}O₇
- 5 Ca_{0.79}Gd_{0.16}U_{0.11}Th_{0.03}Hf_{0.76}Ti_{2.08}O₇.

Electron diffraction patterns showed that the crystals consist of a mixture of polytypes and have extensive twinning and stacking disorder. The main polytypes are 2M and 4M. The latter polytype appears to be more prevalent in the crystals with higher Gd, Th, and U. The diffraction patterns exhibit a Bragg spot at 0.563 nm, consistent with the (002) reflection of zirconolite 2M. Thus, zirconolite 2M is probably the phase responsible for the 0.557 nm peak observed by XRD. However, the calculated intensity of this reflection is very weak (I/Imax ~ 2%), suggesting that preferred orientation may also be a contributing factor to the intensity variations observed by XRD. Calculated diffraction patterns for pyrochlore, brannerite, and rutile were also examined. None of these phases have a reflection close enough to 0.557 nm to explain the XRD results.

4 Work in Progress

Quantitative XRD will be carried out on additional selected samples. Preliminary work (Appendix G) gave a reasonable correlation with Image Analysis methods. It is planned to carry out some additional XRD work on some of the earlier samples.

Work on the identification of the phases in the zirconolite-rich samples is also continuing.

5 Conclusions

Generally, the formulations formed the phases expected. The exception was the nominally ~ 10 % perovskite batch, which did not form perovskite:

- The baseline ceramics, essentially formed pyrochlore as the main phase with 10 20 vol. % brannerite and 3 5 vol. % Hf-doped rutile.
- The baseline + impurities ceramics formed mainly pyrochlore plus ~ 15 vol % 2M zirconolite, ~ 10 20 brannerite, 2 3 vol. % Hf-doped rutile and ~ 2 vol. % of an intergranular silicate glassy phase. The impurities lead to grain growth probably via liquid phase sintering.
- The zirconolite rich ceramics formed an approximately equal mixture of zirconolite and pyrochlore with $\sim 15-20$ vol. % brannerite and sometimes a little (< 5 vol. %) Hf-doped rutile
- The brannerite-rich samples consist of an approximately equal mixture of brannerite and pyrochlore; sometimes $\sim 2-3$ vol. % Hf-doped rutile was present.
- The nominally ~ 10 % perovskite samples had no perovskite with the additional Ca being accommodated in the pyrochlore; as a result pyrochlore formed at the expense of brannerite. Brannerite formed when the sample was sintered in air.
- The phosphate doped samples typically consisted mainly of pyrochlore with 15 20 vol. % brannerite, 5 10 vol. % whitlockite and 1 5 vol. % Hf-doped rutile. The whitlockite (nominally, Ca₃(PO₄)₂) contains Gd, Hf, U, Th and Ti.

Traces (< 1 vol. %) of ThO₂ and PuO₂ were found in some samples. Sometimes this was "unreacted" ¹⁶ and other times it was partly "reacted". By "reacted" we mean that the actinide oxide contained significant amounts of the other elements present in the sample (e.g., Ca, Gd, Hf, U, Ti).

The Pu, U and Th partition as expected – mainly into the pyrochlore, brannerite and zirconolite, with some in the whitlockite and rutile. The amounts in the minor phases, rutile and whitlockite, are small however, and the neutron absorbers Hf and Gd can be found in significant amounts in these phases.

-

¹⁶ The term "unreacted" applies, in this work, to lumps of residual material that have not reacted during sintering.

Some deficiency in rutile around large pores and in a thin surface region (~ $20~\mu m$) of the pellet were observed in the Th/U-doped baseline and zirconolite-rich samples. Some minor preferred orientation effects were observed in the XRD patterns of some of the Th-doped samples. A peak at ~ 0.56~nm was observed in the Th-doped samples that contained zirconolite. This peak was more intense on XRD patterns of the surface of the pellets and appeared in both air and Ar sintered pellets.

Apart from these two observations, no major differences were observed between the surfaces and interior of pellets.

EDS analysis of the interior and exterior regions of a pellet cross section was carried out on several samples of each of the six Th/U-doped compositions tested. These had been sintered in air and Ar, processed via wet and dry ball milling and attrition milling routes. Several Pu/U-doped compositions were also tested. No significant differences were observed in the EDS analyses across any of these pellets.

6 Acknowledgments

Thanks are due to Mr. S. Leung for his help with the SEM/EDS analysis and Mr A. Brownscombe for preparing the Pu-doped samples. We also thank Ms. M.L. Carter for helping out with some of the laboratory work and Dr. C. J. Ball and Mr G. Thorogood for their help with the XRD work.